Articles

Highly Effective Poly(Ethylene Glycol) Architectures for Specific Inhibition of Immune Receptor Activation†

Emily J. Baird,‡ David Holowka, Geoffrey W. Coates,* and Barbara Baird*

Department of Chemistry and Chemical Biology, Cornell University, Ithaca, New York 14853-1301

Received May 27, 2003; Revised Manuscript Received September 4, 2003

ABSTRACT: Architectural features of synthetic ligands were systematically varied to optimize inhibition of mast cell degranulation initiated by multivalent crossing of IgE−receptor complexes. A series of ligands were generated by end-capping poly(ethylene glycol) (PEG) polymers and amine-based dendrimers with the hapten 2,4-dinitrophenyl (DNP). These were used to explore the influence of polymeric backbone length, valency, and hapten presentation on binding to anti-DNP IgE and inhibition of stimulated activation of RBL cells. Monovalent $MPEG_{5000}$−DNP (IC_{50} = 50 nM), bivalent DNP−PEG_{3350}−DNP (IC_{50} = 8 nM), bismonovalent $MPEG_{5000}$−DNP_2 (IC_{50} = 20 nM), bisbivalent DNP_2−PEG_{3350}−DNP_2 (IC_{50} = 3nM) and DNP_4−dendrimer ligands (IC_{50} = 50 nM) all effectively inhibit cellular activation caused by multivalent antigen, DNP−bovine serum albumin. For different DNP ligands, we provide evidence for more effective inhibition due to (i) preferential formation of intra-IgE cross-links by bivalent ligands of sufficient length, (ii) self-association of monovalent ligands with longer tails, and (iii) higher probability of binding for bisvalent ligands. We also show that larger DNP_{16}−dendrimers of higher valency trigger degranulation by cross-linking IgE−receptor complexes, whereas smaller DNP−dendrimers are inhibitory. Thus, features of synthetic ligands can be manipulated to control receptor occupation, aggregation, and inhibition of the cellular response.

Ligand-mediated receptor clustering that stimulates cell signaling is ubiquitous in biological systems (*1*, *2*). Processes ranging from viral entry into a host cell to antigen-induced initiation of signal transduction in the immune response are governed by the formation of cross-links with multiple receptor−ligand bonds. Because naturally occurring ligands are often structurally heterogeneous, defined synthetic ligands provide a valuable tool to investigate important receptor−ligand interactions. The architectural features of a ligand determine the mechanism by which it acts, and synthetic ligands can be tuned either to *mimic* the activity of natural substances that induce a cellular response or to *inhibit* these interactions (*3*, *4*). The prevalence of cellular responses governed by receptor−ligand interactions provides the motivation for the rational design and synthesis of both effectors and inhibitors to understand and manipulate binding events.

A well-studied example is the activation of mast cells that occurs to initiate an allergic immune response when multivalent antigen cross-links IgE antibodies bound to high affinity receptors, FcϵRI, on the cell surface. This antigen-mediated clustering of receptors leads to phosphorylation of tyrosine-based activation motifs within FcϵRI β and γ subunits by the Src family kinase, Lyn (*5*). Receptor phosphorylation, in turn, initiates a signaling cascade that involves an adaptor protein LAT and culminates in secretion of mediators of allergy and inflammation. The main purpose of the present study was to create ligands that prevent antigen-mediated clustering of IgE−FcϵRI complexes and thereby inhibit this immune response. Previous studies have established that multivalent ligands typically are effective triggers, whereas monovalent ligands do not cause cell activation (*6*). Bivalent ligands, however, can cross-link either *intermolecularly*, often leading to productive signaling (*7*, *8*) or *intramolecularly*, which precludes intermolecular cross-linking and thereby inhibits cellular activation (*9*) (Figure 1). An inhibitory bivalent ligand that preferentially interacts with the two antigen binding sites on the same IgE antibody would be beneficial both as a tool in exploring aspects of cellular activation in immune responses and as a potential drug in the treatment of specific allergies. Unfortunately, the structural properties of ligands that are optimal for intramolecular cross-linking are not readily predictable from simple considerations of enthalpy and entropy changes, especially

† This work was supported by NIH Grant AI22449 and the Cornell Nanobiotechnology Center (NSF STC, ECS-9876771) and made use of facilities of the Cornell Center for Materials Research (NSF MRSEC, DMR-0079992). G.W.C. gratefully acknowledges a David and Lucile Packard Foundation Fellowship in Science and Engineering, an Alfred P. Sloan Research Fellowship, an Arnold and Mabel Beckman Foundation Young Investigator Award, and a Camille Dreyfus Teacher−Scholar Award.

* Corresponding authors (bab13@cornell.edu; gc39@cornell.edu).

‡ Current address: The Johns Hopkins School of Medicine, Baltimore, MD.

10.1021/bi034884l CCC: $25.00
Published on Web 10/14/2003

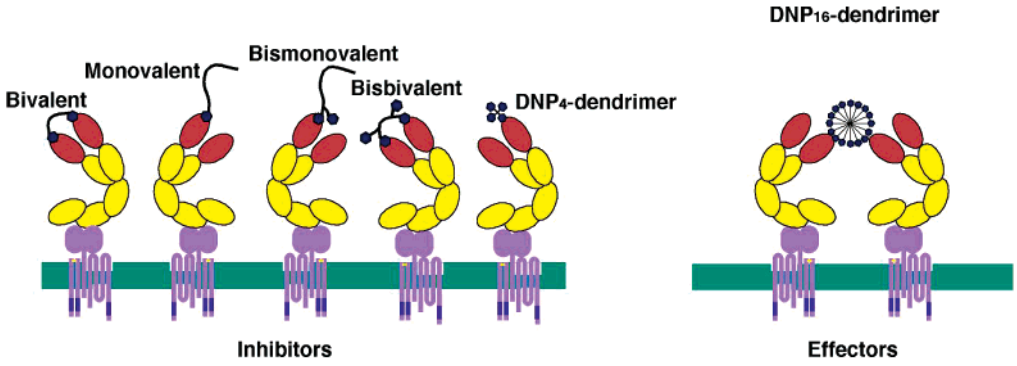

FIGURE 1: DNP ligands with varying architectures and their likely interactions with anti-DNP IgE bound to FcεRI on RBL mast cells.

Scheme 1: Synthesis of Bivalent (DNP−PEG−DNP) and Monovalent (MPEG−DNP) Ligands

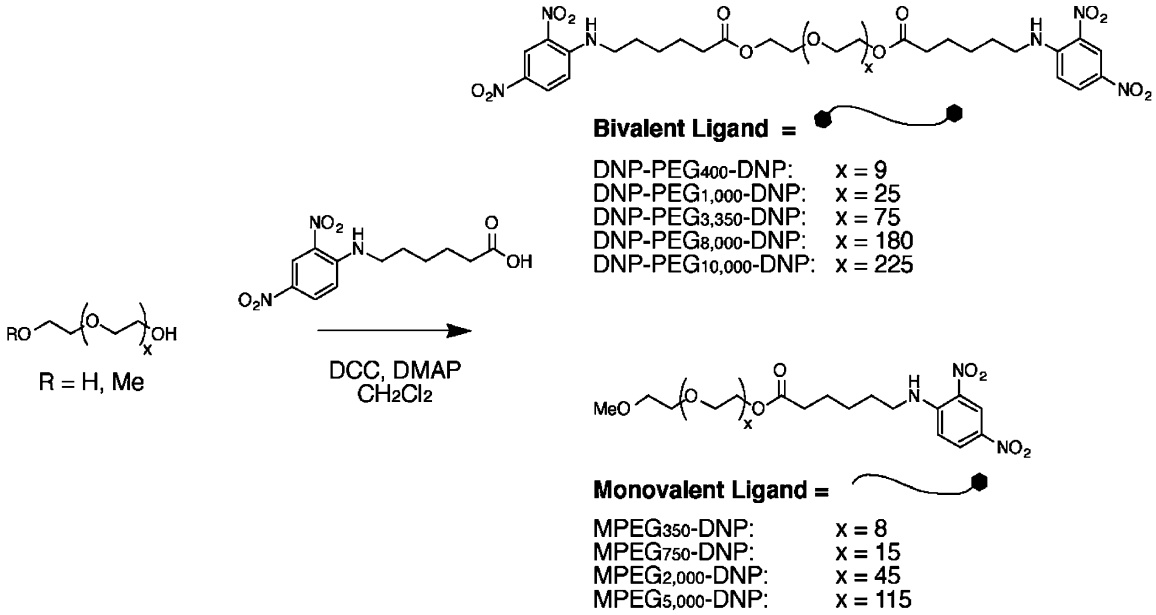

when both binding partners are flexible. However, rational design combined with experimental evaluation can provide general guidelines.

Covalent attachment of a specific group to a polymeric backbone is a useful method for controlling the size, solubility, and biocompatibility without eliminating biological activity (*10*). In recent years, poly(ethylene glycol) (PEG)[1] has emerged as an especially attractive polymer in conjugation chemistry related to biomedical application. Its highly hydrated structure in aqueous solution results in high solubility and exclusion of other macromolecules (*11*, *12*). Capitalizing on PEG's unique aqueous properties has led to a number of useful applications: (i) immobilization of PEG on the surfaces of biomaterials reduces nonspecific protein adsorption (*13*, *14*); (ii) attachment of PEG to the outer surface of proteins decreases immunogenicity and antigenicity (*15*, *16*); (iii) synthesis of PEG liposomes and micelles increases plasma lifetimes (*17*, *18*); (iv) modification of drugs and small molecules with PEG decreases toxicity and increases solubility (*19*); (v) tethering ligands with PEG facilitates interactions with multivalent proteins (*20*).

Because of the success of PEG in biomedical conjugations, this polymer was used as the basis of our ligand design. PEG polymers were terminated with 2,4-dinitrophenyl (DNP) groups to investigate the influence of polymer length and valency on the inhibition of anti-DNP IgE-mediated signaling. Bivalent (DNP−PEG−DNP), monovalent (MPEG−DNP), bismonovalent (MPEG−DNP_2), and bisbivalent (DNP_2−PEG−DNP_2) ligands (Figure 1; Schemes 1 and 2) were synthesized and evaluated for their capacity to inhibit the cross-linking of anti-DNP IgE-FceRI mediated by a potent multivalent antigen. DNP−dendrimers were also evaluated. Because many biological events are initiated by clustering of cell surface receptors, a similar approach can be taken to design modulators of other cellular responses.

MATERIALS AND METHODS

Synthesis and Characterization of Poly(Ethylene Glycol) Ligands. ACS grade methylene chloride and tetrahydrofuran were used as received. Procedures for synthesis of each type of compounds are described below. Gel permeation chromatography was performed using Bio-Beads S-X1 beads (200−400 mesh, Bio Rad). ^{1}H NMR spectra were recorded on a 300 MHz Bruker AF300 spectrometer; physical characteristics and spectral information for all compounds are included in Supporting Information.

[1] Abbreviations: DNP, 2,4-dinitrophenyl; DNP−BSA; bovine serum albumin multiply conjugated with DNP; PEG, poly(ethylene glycol); MPEG, methyl ether PEG; DCC, dicyclocarbohexylcarbodiimide; DMAP, 4-(dimethylamino)pyridine.

Scheme 2: Synthesis of Bisvalent ($DNP_2-PEG-DNP_2$) and Bismonovalent ($MPEG-DNP_2$) Ligands

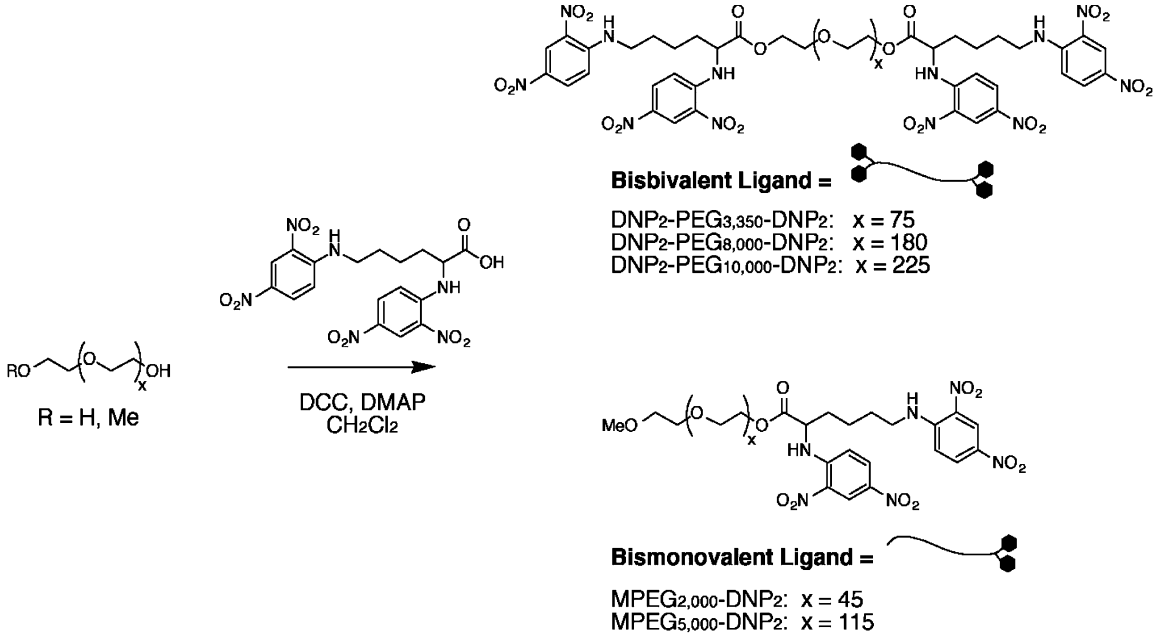

Di(N-2,4-DNP-ϵ-Amino Caproate)−PEG (DNP−PEG$_x$−DNP). Poly(ethylene glycol)s (PEG; Aldrich) of different polymer weights (PEG$_x$) were dried under vacuum for 4 h at 50 °C. To a solution of PEG (0.05 mmol) in 5 mL of methylene chloride, *N*-2,4-DNP-ϵ-amino caproic acid (Sigma) (0.25 mmol), dicyclocarbohexylcarbodiimide (DCC; Aldrich) (0.15 mmol), and 4-(dimethylamino)pyridine (DMAP; Aldrich) (0.005 mmol) were added. The reaction mixture was stirred at room temperature for 12 h. Then the mixture was filtered, and the product was isolated from the filtrate by gel permeation chromatography using THF as the eluant.

(N-2,4-DNP-ϵ-Amino Caproate)−xMPEG (MPEG$_x$−DNP). Poly(ethylene glycol) methyl ether (MPEG; Aldrich) was dried under vacuum for 4 at 50 °C. To a solution of MPEG (0.05 mmol) in 5 mL of methylene chloride, *N*-2,4-DNP-ϵ-amino caproic acid (0.15 mmol), DCC (0.07 mmol), and DMAP (0.005 mmol) were added. Reaction and purification were performed as described above for DNP−PEG$_x$−DNP.

*Bis(N,N′-di(2,4-DNP-*L*-Lysine))−PEG (DNP$_2$−PEG$_x$−DNP$_2$).* PEG was dried under vacuum for 4 h at 50 °C. To a solution of PEG (0.05 mmol) in 5 mL of methylene chloride, *N*,*N*′-di(2,4-DNP-L-lysine) (Sigma) (0.25 mmol), DCC (0.15 mmol), and DMAP (0.005 mmol) were added. Reaction and purification were performed as described above for DNP−PEG$_x$−DNP.

*(N,N′-di(2,4-DNP-*L*-Lysine)−MPEG (MPEG$_x$−DNP$_2$).* MPEG was dried under vacuum for 4 h at 50 °C. To a solution of MPEG (0.05 mmol) in 5 mL of methylene chloride, *N*,*N*′-di(2,4-DNP-L-lysine) (0.25 mmol), DCC (0.15 mmol), and DMAP (0.005 mmol) were added. Reaction and purification were performed as described above for DNP−PEG$_x$−DNP.

Synthesis of (N-2,4-DNP-ϵ-Amino Caproate)-Modified DAB-AM-x Dendrimers (DNP$_x$-Dendrimers). Polypropyleneimine tetramine dendrimer (DAB-AM-4), polypropyleneimine octamine dendrimer (DAB-AM-8), or polypropyleneimine hexadecamine dendrimer DAB-AM-16 (Aldrich) were dried under vacuum overnight at 50 °C. To a solution of DAB-AM-4 (0.1 mmol) in 10 mL of methylene chloride, *N*-2,4-DNP-ϵ-amino caproic acid (0.5 mmol), DCC (0.5 mmol), and DMAP (0.01 mmol) were added. The reaction stirred at room temperature for 12 h. The product was filtered and washed several times with methylene chloride. Reactions with DAB-AM-8 and DAB-AM-16 were carried out similarly with *N*-2,4-DNP-ϵ-amino caproic acid added in a 1.25:1 molar ratio of DNP to amino groups on each dendrimer.

Degranulation Assay. RBL-2H3 cells (*21*) sensitized with purified anti-DNP IgE were incubated at 37 °C overnight in a 48-well plate at a density of 10^6 cells/well. Degranulation measured as β-hexosaminidase release was stimulated by a multivalent antigen (bovine serum albumin, conjugated with about 16 DNP groups; DNP−BSA) or by other DNP ligands, as previously described (*22*). For inhibition studies, a 45-min preincubation of the cells with the inhibitor ligand solutions was followed by an additional 45-min incubation with DNP−BSA at indicated concentrations.

Equilibrium Binding of DNP Ligands to FITC-Modified IgE. Steady-state fluorescence measurements were made with an SLM 8000C fluorescence spectrophotometer in time-based acquisition mode. For each experiment, fluorescein-isothiocyanate (FITC)-modified anti-DNP IgE in 2 mL of buffered saline solution containing BSA (BSA/BSS: 20 mM Hepes, pH 7.4, 135 mM NaCl, 5 mM KCl, 1.8 mM $CaCl_2$, 1 mM $MgCl_2$, 5.6 mM glucose, and 1 mg/mL BSA) was stirred continuously in an acrylic cuvette and thermostatically controlled at 37 °C. FITC was excited at 490 nm, and emission was monitored at 520 nm. Indicated concentrations of DNP−PEG−DNP and MPEG−DNP solutions were added, and specific binding to IgE was monitored as FITC quenching as previously described (*23*).

In Vivo Tyrosine Phosphorylation Assay. RBL-2H3 cells were sensitized with anti-DNP IgE and plated into a 24-well plate (10^6 cells/well). Following overnight incubation at 37 °C, cells were incubated with 1−100 nM of DNP ligands for 10 min, and whole cell lysates were evaluated for phosphorylated protein bands with 4G10 anti-phosphotyrosine antibodies on Western blots as previously described (*24*).

Table 1: Estimated and Experimentally Determined Values for DNP Ligands[a]

ligand	solution length[a] (Å)	extended length[b] (Å)	end valency[c]	molecular valency[d]	degranulation	IC_{50}[e] [nM]
		Bivalent Ligands				
DNP−PEG_{400}−DNP	18	50	1	2	no	202 ± 13
DNP−PEG_{1000}−DNP	28	110	1	2	no	61 ± 7
DNP−PEG_{3350}−DNP	52	290	1	2	no	8 ± 2
DNP−PEG_{8000}−DNP	79	675	1	2	no	10 ± 2
DNP−PEG_{10000}−DNP	92	840	1	2	no	12 ± 5
		Bisbivalent Ligands				
DNP_2−PEG_{3350}−DNP_2	52	290	2	4	no	3 ± 1
DNP_2−PEG_{8000}−DNP_2	79	675	2	4	no	5 ± 1
DNP_2−PEO_{10000}−DNP_2	92	840	2	4	no	7 ± 2
		Monovalent Ligands				
$MPEG_{350}$−DNP	15	20	1	1	no	300 ± 50
$MPEG_{350}$−DNP	17	40	1	1	no	316 ± 24
$MPEG_{750}$−DNP	24	70	1	1	no	250 ± 50
$MPEG_{2000}$−DNP	39	170	1	1	no	195 ± 9
$MPEG_{5000}$−DNP	62	430	1	1	no	51 ± 11
		Bismonovalent Ligands				
$MPEG_{2000}$−DNP_2	39	170	2	2	no	60 ± 12
$MPEG_{5000}$−DNP_2	62	430	2	2	no	19 ± 2
		DNP−dendrimers				
DNP_4−dendrimer	N/A[f]	44	N/A	4	no	50 ± 10
DNP_8−dendrimer	N/A	54	N/A	8	no	300 ± 50
DNP_{16}−dendrimer	N/A	64	N/A	61	yes	N/A

[a] Average end-to-end length of each ligand was estimated from a random walk model, rms length = 5.6 $(N)^{0.5}$. [b] Extended lengths of DNP ligands determined using the MacSpartan modeling program. [c] End valency refers to the number of haptens at one end of the polymer (see Schemes 1−3). [d] Molecular valency refers to the overall valency of the ligand. [e] IC_{50} values are averages (± std dev) from three or more inhibition experiments. [f] Not applicable.

Confocal Fluorescence Microscopy. RBL-2H3 cells were cultured and sensitized in MatTek wells with anti-DNP IgE conjugated with Alexa-488 (Molecular Probes). Labeled cells were treated with ligands as indicated in the figure legend and fixed immediately in 4% formaldehyde/phosphate buffered saline. Confocal images were acquired with an MRC 600 (Bio Rad; excitation at 488 nm, green fluorescence) as previously described (*25*).

RESULTS AND DISCUSSION

Synthesis of PEG-Based DNP Ligands. The primary objective of our study was to determine architectural features of ligands that enhance their capacity to occupy the sites of a bivalent receptor (anti-DNP IgE) and thereby their capacity to inhibit binding and cellular activation caused by an antigen that is an effective intermolecular cross-linker (DNP−BSA). To investigate the roles of valency and polymeric spacer length, a series of PEG-based ligands were synthesized (Table 1). Monovalent (MPEG−DNP) and bivalent (DNP−PEG−DNP) ligands were generated by coupling *N*-2,4-DNP-ϵ-amino-*n*-caproic acid to a series of methoxy-PEG (MPEG) and PEG, respectively (Scheme 1). Covalent attachment of MPEG and PEG to *N*,*N*′-di(2,4-DNP)-L-lysine produced bismonovalent (MPEG−DNP_2) and bisbivalent (DNP_2−PEG−DNP_2) ligands in a range of molecular weights (Scheme 2). All of the ligands were synthesized using DCC coupling. The extent of end-functionalization and purity were determined by ^{1}H NMR and gel-permeation chromatography. The polydispersity of the commercially available PEG employed in these studies is less than 1.05, such that integration of the DNP peaks versus the PEG backbone peaks could be used to establish the degree of end-modification (*26*). Spectroscopic data are provided in Supporting Information.

Inhibition Properties of Bivalent Ligands as a Function of the Length of the PEG Spacer. A bivalent ligand with an appropriate polymeric spacer can cross-link the two antigen binding sites on a single IgE (Figure 1). Although less structurally flexible than the IgG class of immunoglobulins (*27*), the distance between the two antigen binding sites on IgE has some variability. Resonance energy transfer between these sites on IgE provide a rough estimate for the average distance, ∼100 Å (*28*). Bivalent ligands with polymeric spacers that readily span the distance between the two IgE binding sites could potentially form very stable intramolecular cross-links and thereby effectively inhibit mast cell activation caused by an intermolecular cross-linker. To investigate the effect of length on binding to anti-DNP IgE, a series of bivalent DNP ligands with molecular masses ranging from 400 to 10 000 Da were generated (Scheme 1). The average end-to-end length (root-mean-square) of these polymers, estimated from an unrestricted random walk model (*29*−*31*), as well as extended length estimates from molecular modeling are included in Table 1. The wide range of the estimated length from random coil to extended chain (e.g., 52−290 Å for DNP−PEG_{3350}−DNP) suggests the potential flexibility of the PEG spacer.

Because our primary goal was to develop specific inhibitors, control experiments were initially conducted to test whether the bivalent DNP ligands initiate cellular activation by intermolecular cross-linking of cell surface IgE−FcϵRI complexes. For this purpose, RBL mast cells sensitized with anti-DNP IgE were tested with each of the DNP ligands listed in Table 1 (Scheme 1). Stimulated exocytotic release of the granule marker, β-hexosaminidase, was measured. Under conditions in which multivalent DNP−BSA stimulates a maximal response of ∼60% granular release, none of the PEG-based ligands stimulate degranulation significantly

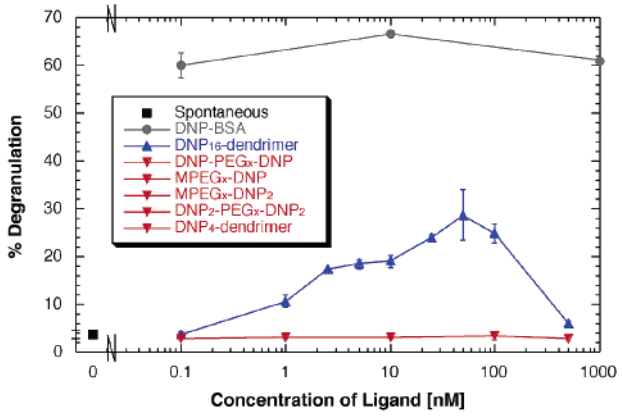

FIGURE 2: Degranulation of RBL cells sensitized with anti-DNP IgE and incubated with DNP ligands for 1 h at 37 °C. Exocytotic release of the granule marker β-hexosaminidase was used to quantify the extent of degranulation. A small amount of spontaneous release (■) occurs with cells that are not stimulated. Strong release is stimulated by multivalent antigen DNP−BSA (●). All DNP ligands in Table 1 were tested, and only DNP_{16}−dendrimer (▲) exhibited release greater than spontaneous. Data from all others are represented by one symbol (▼).

(Figure 2). This is similar to previous results with another synthetic bivalent ligand, *N*,*N*′-bis(DNP-caproyl-L-tyrosyl)-L-cysteine, which has an extended length of ∼50 Å. This ligand cannot form intramolecular cross-links with IgE, but instead cross-links intermolecularly to form highly stable cyclic dimers of IgE−FcϵRI on the cell surface that also fail to stimulate degranulation (*32*). In contrast, bivalent DNP ligands based on a double-stranded DNA spacer do stimulate degranulation when the rigid spacer length is 45−50 Å but not 70−100 Å, although all of these DNA-ligands initiate the first steps of signaling (*4*). These various results illustrate the general difficulty of predicting effects of antigen structure on receptor mediated cellular function, and they also point to the dependence of transmembrane signaling on those structural features. As described below, multivalent dendrimeric DNP ligands also exhibit varying capacity to stimulate degranulation, and this is illustrated in Figure 2 for two different dendrimers, DNP_4−dendrimer and DNP_{16}−dendrimer.

To determine whether the DNP ligands of Table 1 initiate the early signaling steps of receptor tyrosine phosphorylation, we carried out Western blot analyses on lysates of mast cells after incubation with representatives of these ligands. Our results indicate that even the oligovalent DNP−PEG−DNP and DNP_4−dendrimer ligands fail to stimulate the earliest steps in cell activation: enhanced phosphorylation of FcϵRI β subunit and the signaling adaptor protein LAT (Figure 3).

The capacities of the different bivalent DNP−PEG−DNP ligands to inhibit degranulation was assessed by preincubating anti-DNP IgE-sensitized RBL cells with these ligands and subsequently introducing multivalent DNP−BSA. The representative degranulation experiment in Figure 4a shows a striking difference for bivalent ligands with PEG spacers of 3350, 8000, and 10 000 Da compared to those with PEG spacers 1000 and 400 Da. Table 1 summarizes for multiple experiments average IC_{50} values, i.e., the concentrations of the different DNP−PEG−DNP ligands that inhibit 50% of degranulation stimulated by 0.1 nM DNP−BSA. This differential degranulation can be compared with the estimated length range for the DNP−PEG−DNP ligands and the

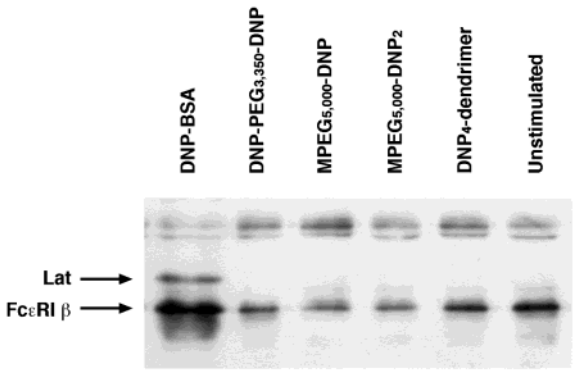

FIGURE 3: Representative Western blot showing tyrosine phosphorylation of LAT and the β-subunit of FcϵRI in RBL cells sensitized with anti-DNP IgE and incubated with 1 nM DNP−BSA or 100 nM DNP−PEG or DNP_4−dendrimer ligands for 10 min at 37 °C. The slightly greater phosphorylation of FcϵRI-β in unstimulated cells compared with that for cells with PEG ligands is not significant in multiple experiments.

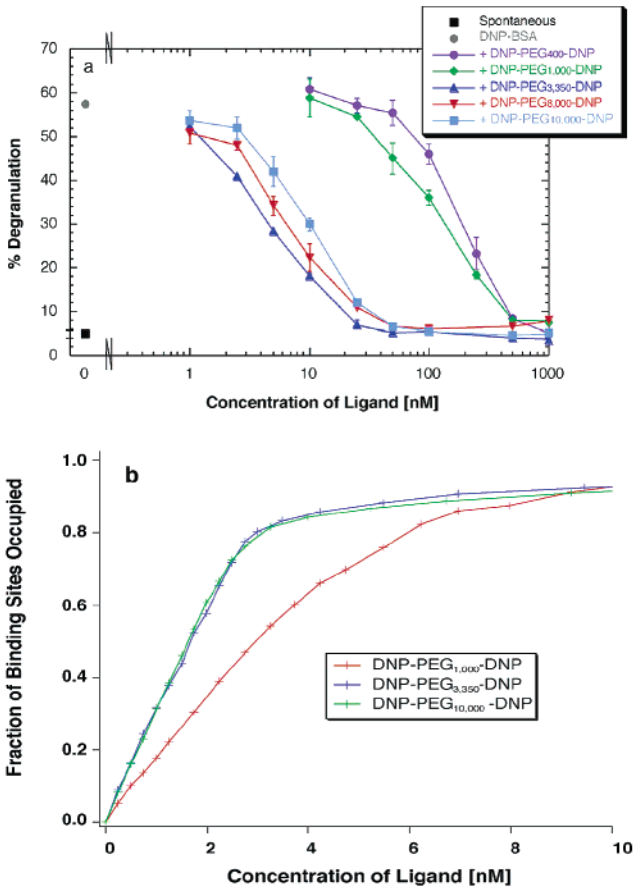

FIGURE 4: (a) Representative results for inhibition of degranulation stimulated by 0.1 nM DNP−BSA with DNP−PEG_x−DNP ligands. A small amount of spontaneous release (■) occurs with cells that are not stimulated. Strong release is stimulated by DNP−BSA in the absence of inhibitors (●). (b) Binding of DNP−PEG_x−DNP ligands to IgE in solution as monitored by fluorescence quenching. A steeper initial slope corresponds to higher apparent affinity.[2]

average distance between the two binding sites on a single IgE (∼100 Å). Potent inhibition (∼10 nM) by the three longer DNP−PEG−DNP ligands correlates with lengths that can span the two IgE binding sites. $DNP-PEG_{1000}-DNP$, which could potentially span this distance in an extended configuration is six times less potent than the longer ligands but inhibits three times better than $DNP-PEG_{400}-DNP$,

which cannot span the distance. Thus, the correlation is consistent with the hypothesis that the longer bivalent ligands can maintain stable, nonstimulatory intramolecular cross-linking on the cell surface in the presence of a competitive multivalent antigen. The trend among the different spacer lengths shown in Figure 4a was observed consistently suggesting that the length of DNP−PEG_{3350}−DNP is most conducive for stable intramolecular cross-linking. However, similar average IC_{50} values for the three longer DNP−PEG−DNP ligands suggests that the flexibility of PEG spacers in this mass range readily allows conformations that attain the minimal free energy associated with bivalent binding in the IgE sites (*33*, *34*).

Equilibrium binding measurements for the bivalent ligands provide further evidence for length-dependent formation of intramolecular cross-links between one bivalent IgE and one bivalent DNP−PEG−DNP ligand of sufficient length. The apparent binding affinities were evaluated by monitoring fluorescence quenching of FITC−IgE in solution upon addition of the ligands under equilibrium conditions (*23*). Binding with higher apparent affinity, *K*, corresponds to a greater initial slope in the fluorescence change.[2] Consistent with the IC_{50} values revealed in the degranulation inhibition assays (Table 1), longer (3350 and 10 000 Da) bivalent ligands exhibit binding with significantly higher apparent affinity compared to DNP−PEG_{1000}−DNP (Figure 4b). Using a simple model, values for $1/K$ (corresponding to an apparent dissociation constant) can be estimated from plots of f (fraction of sites bound) vs $[DNP]_{free}$ as the concentration corresponding to $f = 0.5$.[2] These values are ∼2 nM for DNP−PEG_{1000}−DNP compared to ∼0.07 nM for DNP−PEG_{3350}−DNP and DNP−PEG_{10000}−DNP (plots not shown). The higher apparent affinities for the longer DNP−PEG−DNP ligands cannot be accounted for by intermolecular cross-linking, as indicated by their incapacity to stimulate degranulation (Figure 2) and by gel permeation chromatography of soluble IgE−DNP−PEG−DNP complexes that showed no higher molecular weight species (data not shown). These results support the view that bivalent ligands with a polymeric spacer of appropriate length effectively act as chelates, forming intramolecular cross-links with the two binding sites on a single IgE. As long as one DNP moiety is bound, the diffusion of its tethered DNP is constrained by the effective length of the ligand. Therefore, the probability of binding both ends (the apparent affinity or avidity) for these ligands is increased, and the capacity for competitive inhibition is enhanced.

Our results are consistent with those of Schweitzer-Stenner et al. (*35*) who showed that bivalent DNP ligands with oligoproline spacers in the length range of 130−150 Å form intramolecular cross-links with IgE in solution, whereas bivalent DNP ligands with flexible spacers less than 45 Å form cyclic dimers of IgE. The result that the chelate effect is strong for these long ligands is consistent with structural rigidity expected for oligoprolines and suggests that the PEG spacers also have limited flexibility. Although there appears to be a broad optimal length for intramolecular cross-linking with both types of spacers, we would expect that the apparent chelate effect would be lost as ligand length continues to increase (*9*). A significant difference between DNP−PEG_{3350}−DNP and DNP−PEG_{10000}−DNP is not detected in our simple binding analysis, but an optimum nearer DNP−PEG_{3350}−DNP is suggested by the representative results of Figure 4a. Other potential contributions to the binding behavior are suggested by studies with monovalent MPEG−DNP ligands as described below.

Fluorescence microscopy experiments were performed to visualize changes in IgE−FcϵRI distribution on the cell surface after treatment with various ligands. As shown in Figure 5, unstimulated cells sensitized with Alexa 488-labeled IgE show uniform distribution of IgE−FcϵRI at equatorial (Figure 5a) and top surface confocal planes (Figure 5b). Cells incubated with 1 nM DNP−BSA for 10 min at 25 °C show a patchy distribution of cross-linked IgE−FcϵRI at the cell surface, most evident in the equatorial section (Figure 5c). Also, DNP−BSA treated cells show stimulated protrusions, or ruffling, when the top surface is viewed (Figure 5d) (*25*). In contrast, cells treated with 1 nM DNP−BSA together with 1 μM DNP−PEG_{3350}−DNP for 10 min exhibit complete inhibition of receptor patching (Figure 5e) and stimulated ruffling (Figure 5f), consistent with the inhibition of degranulation (Figure 4a). Cells treated with 1 μM DNP−PEG_{3350}−DNP alone appear the same as unstimulated cells (Figure 5a,b).

Inhibition Properties of Monovalent Ligands as a Function of the Length of the PEG Tail. The lower apparent binding affinities and less potent inhibitory properties of shorter bivalent PEG ligands (400 and 1000 Da) can be explained by insufficient formation of intra-IgE cross-links. However, 3-fold differences in their capacity to inhibit DNP−BSA in degranulation assays (Figure 4a and Table 1) point to significant dependence on PEG spacer length. To investigate inhibition resulting from structural effects of the PEG component, a series of monovalent ligands were synthesized by end-capping MPEG with DNP (Scheme 1). These ligands bind specifically to only one IgE site and correspondingly do not cross-link IgE−FcϵRI on cells (Figure 1), stimulate FcϵRI or LAT phosphorylation (Figure 3) or degranulation (Figure 2). Although all monovalent ligands bind to IgE through the same DNP end group, we consistently observe that inhibition becomes more pronounced as the length of the PEG tail increases, such that $MPEG_{5000}$−DNP is roughly 4-fold more potent than $MPEG_{2000}$−DNP and roughly 6-fold more potent than $MPEG_{350}$−DNP and $MPEG_{130}$−DNP (Figure 6a; Table 1). Previous studies suggest that highly hydrated, cell-associated PEG can physically prevent competing interactions at the cell surface (*33*, *34*). Thus, as the

[2] This analysis is based on the simplest model of protein−ligand binding: P + L = PL; $K = [PL]/[P][L]$ where P corresponds to a free IgE antibody site, L corresponds a free DNP hapten, PL corresponds to the bound complex, K is the affinity constant, and $1/K$ is the dissociation constant. If f = fraction of sites bound, then $f = K[L]/(1 + K[L])$ and $f = 0.5$ corresponds to $[L] = 1/K$. For hyperbolic plots of f vs [L], the initial slope (for small [L]) $= K[L]$. [L] can be determined from total ligand (L_t) and total sites (P_t) concentrations as $[L] = L_t - f P_t$. The ligands examined in this study show more complicated binding behavior than this simple model as described in the text, and we are developing more sophisticated models that parametrize bivalent binding, steric hindrance, and self-association effects (Das, Baird, Holowka, Goldstein, and Baird, manuscript in preparation). However, the simple model is useful for the purposes of making comparisons of relative apparent affinity. Thus, for ligands binding with higher apparent affinity (represented by K), plots of f vs [L] have greater initial slopes and lower values for [L] corresponding to $f = 0.5$. These apparent K average over various possible contributions to the ligand binding, including intramolecular cross-linking, steric hindrance, and self-association.

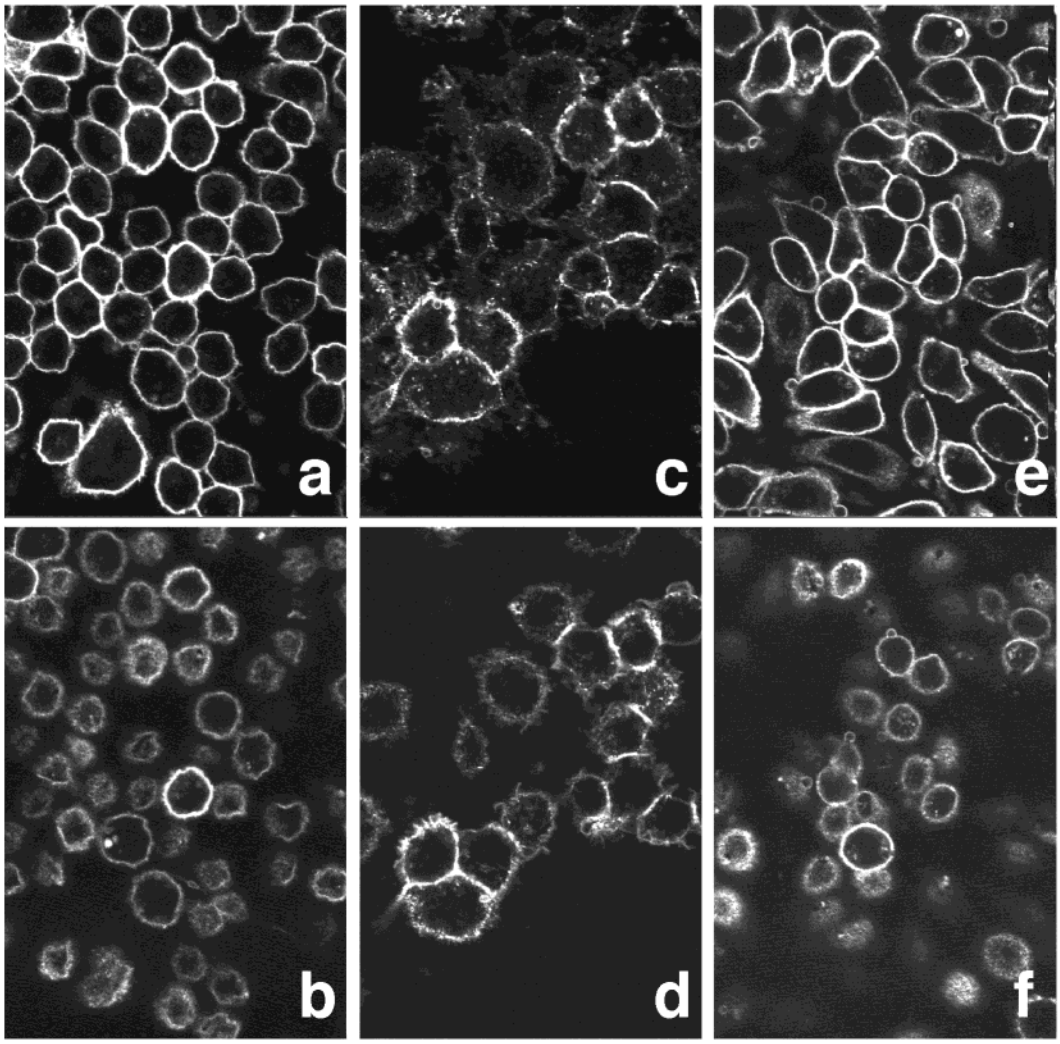

FIGURE 5: Confocal fluorescence images of the equatorial (a, c, e) and top (b, d, f) surface of RBL cells sensitized with Alexa-488 IgE. Cells were incubated without (a, b) or with 1 nM DNP−BSA (c, d), or with 1 nM DNP−BSA together with 1000 nM DNP−PEG_{3350}−DNP (e, f) for 10 min at 25 °C.

length of the PEG tail increases, the polymer may provide a larger obstruction for approaching macromolecules, such as DNP−BSA. In this case, we would also expect to observe a steric inhibitory effect on MPEG−DNP binding.

Equilibrium binding was measured for the monovalent PEG ligands. The relative shapes of the binding curves reveal that apparent affinity for $MPEG_{2000}$−DNP binding is similar to $MPEG_{750}$−DNP. Interestingly, the longest monovalent ligand ($MPEG_{5000}$−DNP) shows markedly higher apparent affinity binding compared to the smaller ligands (Figure 6b). As for the bivalent ligands we estimated values for $1/K$ from a simple model and plots of f vs $[DNP]_{free}$.[2] These values are ∼5 nM for $MPEG_{5000}$−DNP compared to ∼12 nM for $MPEG_{750}$−DNP and $MPEG_{2000}$−DNP (plots not shown). More realistic modeling of these binding data indicate that the longer tails of PEG ligands can interact with competing effects (R. Das, E. Baird, D. Holowka, B. Goldstein, and B. Baird, manuscript in preparation). The inhibitory contribution is probably due to steric hindrance. The unexpected enhancement observed with $MPEG_{5000}$−DNP suggests self-association of two PEG tails that are simultaneously anchored to IgE sites separated by ∼100 Å. This would form a noncovalent bivalent ligand in situ and an intramolecular crosslink. Interactions of closely spaced PEG tails are relevant for many applications of this biocompatible polymer, and ongoing studies are characterizing and quantifying these effects with an extended series of $MPEG_x$−DNP ligands and realistic binding models.

Effects of End-Valency on Inhibition. In addition to ligands with the DNP haptens separated by a PEG spacer, we also examined the influence of terminating each end of the polymer with more than one hapten. "Bismonovalent" (MPEG−DNP_2) and "bisbivalent" (DNP_2−PEG−DNP_2) ligands with *two* DNP groups at one or both ends of PEG, respectively, were synthesized to investigate the influence of end-valency on the inhibitory properties of PEG-based ligands (Scheme 2). Because the spacing between the two DNP groups at one end of these ligands is less than 20 Å, they cannot bind simultaneously to more than one IgE binding site. As expected, these "bisvalent" analogues do not stimulate tyrosine phosphorylation of FcεRI or LAT (Figure 3) or cellular degranulation (Figure 2). Comparison of bismonovalent and bisbivalent ligands with monovalent and bivalent ligands, respectively, show that the bisvalent ligands are more effective inhibitors on a per-molecule basis (Figure 7a,b; Table 1). These results are consistent with the expectation that the bisvalent ligands would have a statistical advantage by a factor of 2 if both DNP groups bind in the

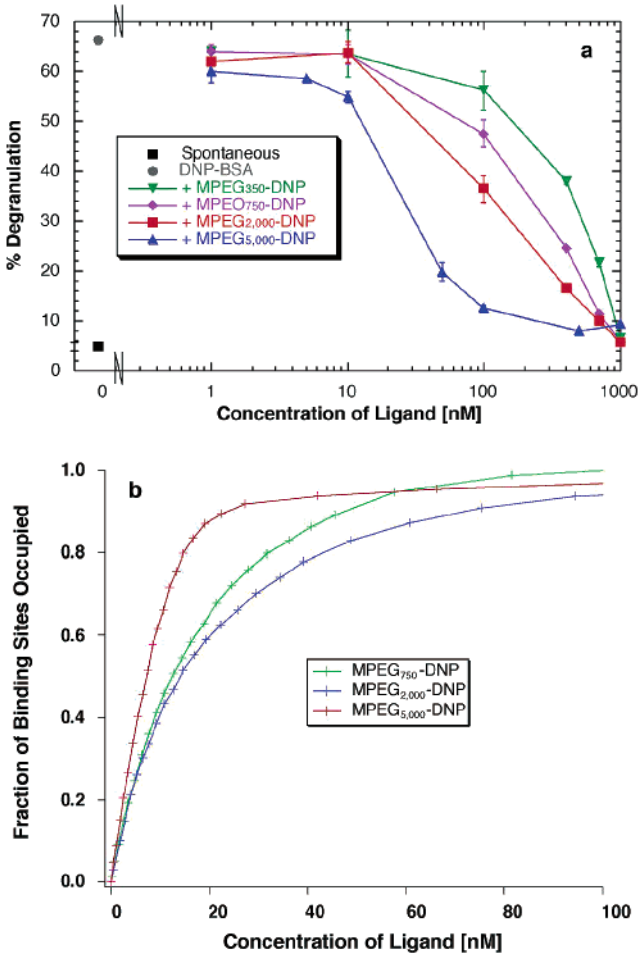

FIGURE 6: (a) Representative results for inhibition of degranulation stimulated by 0.1 nM DNP−BSA with $MPEG_x$−DNP ligands. A small amount of spontaneous release (■) occurs with cells that are not stimulated. Strong release is stimulated by DNP−BSA in the absence of inhibitors (●). (b) Binding of $MPEG_x$−DNP ligands to IgE in solution as monitored by fluorescence quenching. A steeper initial slope corresponds to higher apparent affinity.[2]

IgE sites with the same intrinsic affinity. Other contributions to the enhanced inhibition may also be involved as the additional DNP group is on a shorter chain and might be expected to bind with lower affinity (Scheme 2).

Stimulatory and Inhibitory Properties DNP_x-Dendrimers. To investigate further the relationship between valency and ligand activity, DNP_n−dendrimers were synthesized by coupling DNP to amine-based dendrimers (*36*) (Scheme 3). Three different generations of DNP_n−dendrimers were synthesized and named according to the number of surface DNP groups (e.g., DNP_4−dendrimer).

The efficiency of DNP_x−dendrimer for stimulating degranulation correlates with generation-dependent increases in volume and valency. Only the third generation DNP_{16}−dendrimer shows significant stimulatory activity (Figure 2, Table 1). The failure of DNP_4−dendrimer and DNP_8−dendrimer to stimulate degranulation indicates that they are inefficient at cross-linking cell surface IgE despite their multivalency. The larger diameter and higher valency of DNP_{16}−dendrimer facilitates this interaction to cause cell activation. The biphasic nature of the dose−response curve for this ligand is typical for smaller oligovalent ligands (*4*, *22*). The decreased response at high doses of ligand is due to predominating monovalent binding and/or to desensitization. Extending the valency of this series of ligands may increase the magnitude of the cellular response.

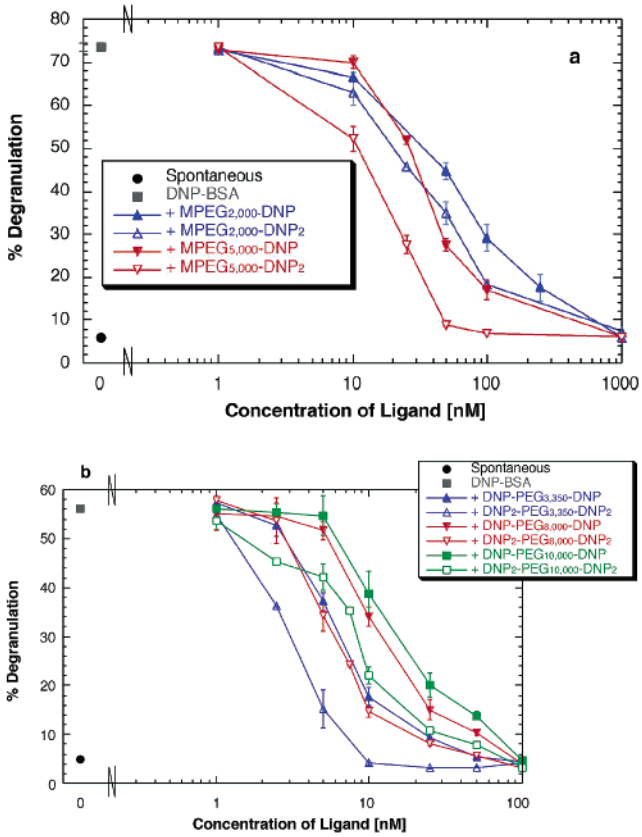

FIGURE 7: Representative results for inhibition of degranulation stimulated by 0.1 nM DNP−BSA, comparing (a) $MPEG_x$−DNP with $MPEG_x$−DNP_2 ligands and (b) DNP−PEG_x−DNP with DNP_2−PEG_x−DNP_2 ligands. A small amount of spontaneous release (■) occurs with cells that are not stimulated. Strong release is stimulated by DNP−BSA in the absence of inhibitors (●).

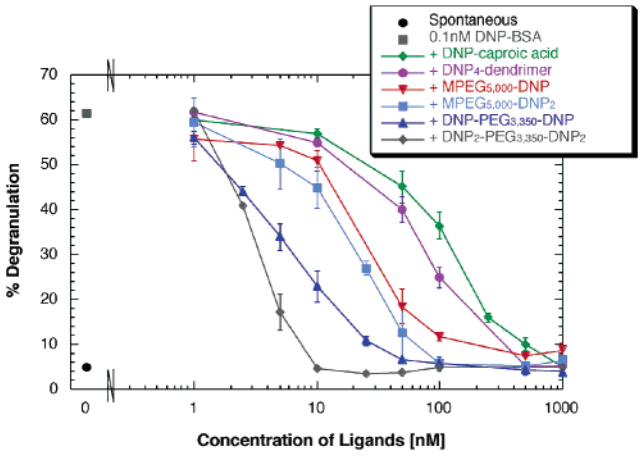

FIGURE 8: Representative results for inhibition of degranulation stimulated by 0.1 nM DNP−BSA, comparing a variety of DNP−PEG and DNP−dendrimer ligands. A small amount of spontaneous release (■) occurs with cells that are not stimulated. Strong release is stimulated by DNP−BSA in the absence of inhibitors (●).

The inhibitory properties of the smaller two, nonstimulatory DNP_n−dendrimers are compared to the other types of inhibitory DNP ligands in Figure 8 and Table 1. DNP_4−dendrimer is the only dendrimer-based ligand studied that is a better inhibitor than the monovalent analogue, DNP−caproate. The lesser potency of DNP_8−dendrimers (IC_{50} =

Scheme 3: Structure of DNP_x−Dendrimer Ligands Synthesized by Coupling DNP to Surface Amine Groups of Amine-Based Dendrimers

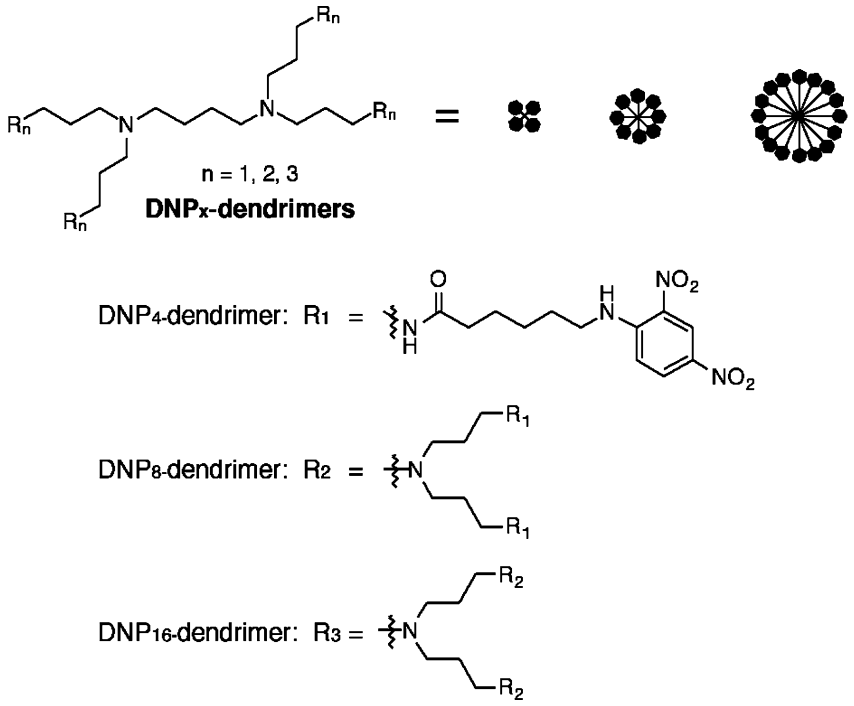

300 nM) compared to DNP_4−dendrimer (IC_{50} = 50 nM) may result from the bulky and sterically hindered nature of this ligand. Increases in valency are accompanied by only slight volume increases, resulting in densely packed DNP groups that may interact and reduce their availability for binding. Thus, the effective ligand valency for binding to IgE may be reduced. The capacity of the DNP_{16}−dendrimer to stimulate degranulation indicates that sufficient hapten binding and intermolecular cross-linking can occur at a sufficiently large radius for these dendritic structures.

CONCLUSIONS

Our systematic investigation of the relationship between the structural features of ligands and their inhibitory properties has led to inhibitors of antigen-stimulated degranulation that are active in the range of 1−300 nM and are as much as 100-fold more potent than small monovalent haptens (Figure 8 and Table 1). Thus, we have demonstrated that the capacity to prevent clustering of IgE−FcϵRI complexes on the cell surface can be tuned via changes in ligand length, overall valency, and end-valency. We anticipate that guidelines emerging from these results will be broadly applicable for rational design of other receptor inhibitors.

The pervasiveness of multivalent ligand−receptor interactions in biological systems is the impetus for exploring the role of ligand architecture in these binding events, and synthetic ligands provide a means to understand and to control these interactions. In this study, we employed a prototypical system for cross-link-dependent receptor signaling and consequent cell activation. The architectural elements of synthetic ligands that competitively inhibit these cross-linking events may have more general relevance for other such receptors. A practical goal for the IgE receptor system is development of potent inhibitors for the treatment of allergies. The inhibitory ligands used are based on PEG because this polymer is being used increasingly in drug development based on its excellent biocompatibility. The most potent inhibitors found are bivalent ligands that form very stable intramolecular cross-links between the two antigen binding sites of IgE. We also found evidence for inhibitory contributions from apparent self-association of the PEG component and from multiple end-valency that could increase the probability of binding. The most potent inhibitor (DNP_2−PEG_{3350}−DNP_2; IC_{50} = 3 nM) is effective at concentrations that are practical for pharmaceutical efficacy. The slow metabolism of PEG (*11*, *18*) further enhances its effectivness in such an application.

In summary, our results demonstrate that ligand architecture can be effectively manipulated for understanding and controlling cell surface binding events. Because many biological events are initiated by clustering cell surface receptors our results can serve as guidelines for designing ligands to modulate other cellular responses. Our ongoing studies are testing these and other types of ligands, and binding data are being fitted with models including parameters for positive (self-association) and negative (steric exclusion) contributions that can be related to functional effects.

ACKNOWLEDGMENT

We thank Dr. Byron Goldstein at Los Alamos National Laboratory and Professor Deborah Leckband at University of Illinois for helpful discussions. Raibatak Das in our laboratory developed computational methods and fitted these binding data with simple and more sophisticated models (manuscript in preparation) yielding parameters that support the conclusions drawn in this paper.

SUPPORTING INFORMATION AVAILABLE

Physical characteristics, yields, and ^{1}H NMR spectral information are included for each of the compounds syn-

thesized and used in this study. This material is available free of charge via the Internet at http://pubs.acs.org.

REFERENCES

1. Metzger, H. (1992) *J. Immunol. 149*, 1477−1487.
2. Mammen, M., Choi, S. K., and Whitesides, G. M. (1998) *Angew. Chem., Int. Ed. 37*, 2755−2794.
3. Kiessling, L. L., Gestwicki, J. E., and Strong, L. E. (2000) *Curr. Opin. Chem. Biol. 4*, 696−703.
4. Paar, J. M., Harris, N. T., Holowka, D., and Baird, B. (2002) *J. Immunol. 169*, 856−864.
5. Kinet, J. P. (1999) *Annu. Rev. Immunol. 17*, 931−72.
6. Holowka, D., and Baird, B. (1996) *Annu. Rev. Biophys. Biomol. Struct. 25*, 79−112.
7. Kane, P., Erickson, J., Fewtrell, C., Baird, B., and Holowka, D. (1986) *Mol. Immunol. 23*, 783−790.
8. Kane, P., Holowka, D., and Baird, B. (1988) *J. Cell Biol. 107*, 969−980.
9. Archer, B. G., and Krakauer, H. (1977) *Biochemistry 16*, 618−628.
10. Veronese, F. M., and Morpurgo, M. (1999) *Farmaco 54*, 497−516.
11. Monfardini, C., and Veronese, F. M. (1998) *Bioconj. Chem. 9*, 418−450.
12. Zalipsky, S. (1995) *Adv. Drug Del. Rev. 16*, 157−182.
13. Abuchowski, A., Vanes, T., Palczuk, N. C., and Davis, F. F. (1977) *J. Biol. Chem. 252*, 3578−3581.
14. Deible, C. R., Petrosko, P., Johnson, P. C., Beckman, E. J., Russell, A. J., and Wagner, W. R. (1999) *Biomaterials 20*, 101−109.
15. Delgado, C., Francis, G. E., and Fisher, D. (1992) *Crit. Rev. Ther. Drug Carrier Syst. 9*, 249−304.
16. Nucci, M., Shorr, R., and Abuchowski, A. (1991) *Adv. Drug Delivery Rev. 6*, 133−151.
17. Lynn, D. M., Amiji, M. M., and Langer, R. (2001) *Angew. Chem., Int. Ed. 40*, 1707−1710.
18. Woodle, M. C., and Lasic, D. D. (1992) *Biochim. Biophys. Acta 1113*, 171−199.
19. Greenwald, R. B., Conover, C. D., and Choe, Y. H. (2000) *Crit. Rev. Ther. Drug Carrier Syst. 17*, 101−161.
20. Kramer, R. H., and Karpen, J. W. (1998) *Nature 395*, 710−713.
21. Barsumian, E. L., Isersky, C., Petrino, M. G., and Siraganian, R. P. (1981) *Eur. J. Immunol. 11*, 317−323.
22. Harris, N. T., Goldstein, B., Holowka, D., and Baird, B. (1997) *Biochemistry 36*, 2237−2242.
23. Erickson, J., Kane, P., Goldstein, B., Holowka, D., and Baird, B. (1986) *Mol. Immunol. 23*, 769−781.
24. Sheets, E. D., Holowka, D., and Baird, B. (1999) *J. Cell Biol. 145*, 877−87.
25. Holowka, D., Sheets, E. D., and Baird, B. (2000) *J. Cell Sci. 113*, 1009−1019.
26. Katre, N. (1993) *Adv. Drug Delivery Rev. 10*, 91−114.
27. Oi, V. T., Vuong, T. M., Hardy, R., Reidler, J., Dangle, J., Herzenberg, L. A., and Stryer, L. (1984) *Nature 307*, 136−140.
28. Baird, B., Zheng, Y., and Holowka, D. (1993) *Acc. Chem. Res. 26*, 428−434.
29. Mattice, W. L., and Carpenter, D. K. (1976) *J. Chem. Phys. 64*, 3261−3265.
30. Yoon, D. Y., and Flory, P. J. (1976) *Macromolecules 9*, 294−299.
31. Sarmoria, C., and Blankschtein, D. (1992) *J. Phys. Chem. 96*, 1978−1983.
32. Posner, R. G., Subramanian, K., Goldstein, B., Thomas, J., Feder, T., Holowka, D., and Baird, B. (1995) *J. Immunol. 155*, 3601−3609.
33. Karlstrom, G., and Engkvist, O. (1997) in *Poly(ethylene Glycol) Chemistry and Biological Application* (Harris, J. M., and Zalipsky, S., Eds.) pp 16−30, American Chemical Society, Washington DC.
34. Lasic, D. (1997) in *Poly(ethylene Glycol) Chemistry and Biological Applications* (Harris, J. M., and Zalipsky, S., Eds.) pp 31−44, American Chemical Society, Washington DC.
35. Schweitzer-Stenner, R., Licht, A., Luscher, I., and Pecht, I. (1987) *Biochemistry 26*, 3602−3612.
36. Liu, M. J., and Frechet, J. M. J. (1999) *Pharm. Sci. Technol. Today 2*, 393−401.

BI034884L